



Elastic electron scattering by tetramethylmethane, tetramethylsilane, and tetramethylgermaneP. A. S. Randi ^{*}, G. M. Moreira [†], and M. H. F. Bettega [‡]*Departamento de Física, Universidade Federal do Paraná, Caixa Postal 19044, 81531-980 Curitiba, Paraná, Brazil*

(Received 3 April 2020; revised 31 May 2020; accepted 20 July 2020; published 14 August 2020)

We report integral, differential, and momentum transfer cross sections for elastic scattering of electrons by tetramethylmethane [C(CH₃)₄], tetramethylsilane [Si(CH₃)₄], and tetramethylgermane [Ge(CH₃)₄]. The scattering cross sections were calculated with the Schwinger multichannel method implemented with pseudopotentials, in the static-exchange and static-exchange plus polarization levels of approximation, for impact energies up to 30 eV. All three molecules present in their integral elastic cross section a broad structure between 5 and 15 eV, which is a superposition of two shape resonances assigned to the E and T_2 symmetries of T_d . The low-energy behavior of the s -wave integral cross section and the s -wave eigenphase support the presence of a Ramsauer-Townsend minimum for C(CH₃)₄ at 0.16 eV, for Si(CH₃)₄ at 0.32 eV, and for Ge(CH₃)₄ at 0.40 eV. In general, the present elastic integral cross sections show a good qualitative agreement with the experimental total cross sections of Stefanowska-Tur *et al.* [*J. Chem. Phys.* **150**, 094303 (2019)].

DOI: [10.1103/PhysRevA.102.022812](https://doi.org/10.1103/PhysRevA.102.022812)**I. INTRODUCTION**

The understanding of the processes and mechanisms that govern the interaction between low-energy electrons and molecules is fundamental to many areas [1]. Secondary non-thermal low-energy electrons produced by the interaction of high-energy radiation in biological and interstellar media play a significant role in radiation induced DNA damage [2,3] and in the syntheses of complex organic molecules in cosmic ices and interstellar dust grains [4,5], respectively. The interactions between electrons and molecules also have an important role in modern technological applications such as focused electron beam induced deposition [6] and plasma assisted material processing [7]. Through these techniques, compounds such as tetramethylsilane [Si(CH₃)₄] and tetramethylgermane [Ge(CH₃)₄] have been used as precursors to prepare deposits of SiO_x [8,9], SiN_x:H [10], Ge_xC_{1-x}:H [11], and Ge_xO_y:H [12] successfully in many academic studies and technological applications. Although electron-molecule interactions play a significant role in those deposition processes, there is a lack of theoretical studies about electron interactions with the X(CH₃)₄ (X = C, Si, Ge) precursors in the low energy regime.

On one hand, many studies on the interaction between electrons and Si(CH₃)₄ have been made. Singlet and triplet excited states of Si(CH₃)₄ and the electron-impact vibration excitation function were obtained using electron energy loss spectroscopy and density-functional theory combined with single configuration interaction (DFT/SCI) calculations by Huber *et al.* [13]. Injection of electrons using a laser photoionization technique enabled Faidas *et al.* [14] to measure electron drift velocities as a function of the applied uniform

electric field in vapor tetramethylmethane [C(CH₃)₄] and liquid and vapor Si(CH₃)₄. Measurements of absolute partial cross sections for the electron impact ionization and dissociative ionization of Si(CH₃)₄ were made by Basner *et al.* [15] employing mass spectrometry techniques. Joshipura and co-workers [16] also have determined the total electron-impact ionization and summed electronic excitation cross section using the complex potential ionization contribution. Using a double-shutter drift tube method with electron arrival-time spectra analysis, Yoshida *et al.* [17] measured the effective ionization coefficient, the mean-arrival-time drift velocity, and longitudinal diffusion coefficient for vapor Si(CH₃)₄. Bordage [18] and Hien *et al.* [19] calculated, using a Boltzmann equation solution and the coefficients measured by Yoshida *et al.* [17], a set of cross sections for Si(CH₃)₄ including the elastic momentum transfer, two vibrational, a total electronic excitation, total attachment, and total ionization cross sections over a wide impact energy range. Kawaguchi *et al.* [20] also determined a set of electron cross sections for Si(CH₃)₄ by the electron swarm method. Sugohara *et al.* [21] investigated the elastic scattering of electrons by Si(CH₃)₄ in the energy range from 100 to 1000 eV. The authors determined the differential, integral, and momentum transfer cross sections for this molecule both experimentally and theoretically using the relative flow technique and the independent atom model and additivity rule, respectively.

On the other hand, only a few studies on these interactions with C(CH₃)₄ and Ge(CH₃)₄ exist. In some of them, some properties of Si(CH₃)₄ were also measured. Electron drift velocity as a function of temperature was measured by McCorkle *et al.* [22] for C(CH₃)₄ and, through these data, they determined the momentum transfer cross section and found a Ramsauer-Townsend (RT) minimum at 0.25 eV. The first derivative with respect to the energy of the transmission current as a function of the incident electron energy was determined by Giordan and Moore [23] through electron

^{*}pasr@fisica.ufpr.br[†]gmm08@fisica.ufpr.br[‡]bettega@fisica.ufpr.br

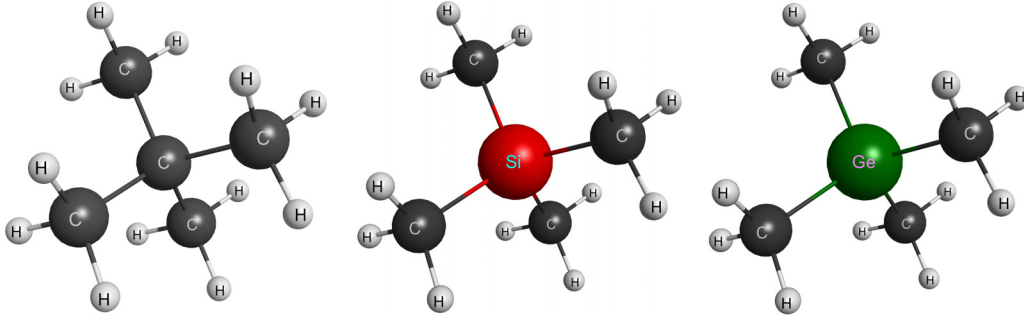


FIG. 1. Ball-and-stick models for $C(CH_3)_4$, $Si(CH_3)_4$, and $Ge(CH_3)_4$. The central atom atomic number increases from the left to the right (generated with MCMOLPLT [26]).

transmission spectroscopy (ETS) for $C(CH_3)_4$, $Si(CH_3)_4$, and $Ge(CH_3)_4$. Modelli *et al.* [24], using the same experimental method (ETS) and *ab initio* and semiempirical calculations, also reported the electron attachment energy of the lowest unoccupied molecular orbitals for $Si(CH_3)_4$ and $Ge(CH_3)_4$.

Aside from the works mentioned above, Stefanowska-Tur *et al.* [25] measured the absolute electron-scattering *grand*-total cross sections (TCS) for $C(CH_3)_4$, $Si(CH_3)_4$, and $Ge(CH_3)_4$ using a linear electron transmission technique with a electrostatic electron spectrometer covering energies from 0.5 to 30 eV. The integral elastic cross section (ICS) and ionization cross section were calculated for intermediate and high impact energies using the additive rule approximation and binary-encounter Bethe approach. The authors reported a large enhancement between 4 and 25 eV in the TCS of these molecules and some other features. While these data give information about the overall electron-molecule interaction, the interpretation of individual features, such as the formation of a transient negative ion and the presence of a RT minimum, requires knowledge of specific cross sections.

In this work, our main goal is to present a reliable set of elastic cross sections for the compounds $X(CH_3)_4$ ($X = C, Si$, and Ge) obtained through *ab initio* electron-molecule collision calculations. The ball-and-stick models for these molecules are shown in Fig. 1 (generated with MCMOLPLT [26]). With these results we can contribute to the cross sections set which is needed for industrial processing and modeling as well as to investigate how the central atom changes the behavior of the cross sections. To this end, we employed the Schwinger multichannel method implemented with pseudopotentials to compute elastic integral, differential, and momentum transfer cross sections for $C(CH_3)_4$, $Si(CH_3)_4$, and $Ge(CH_3)_4$. Our calculations were carried out in the static-exchange and in the static-exchange plus polarization approximations for impact energies up to 30 eV. Our ICSs are compared with the TCS of Stefanowska-Tur *et al.* [25].

The rest of this paper is organized as follows. In Sec. II we present the theory and the computational procedures used in our calculations and in Sec. III we present our results and discussion. A brief summary of our results is presented in Sec. IV.

II. COMPUTATIONAL DETAILS

We optimized the ground state geometry of the three molecules in the T_d point group using density functional

theory (DFT) with the B3LYP exchange-correlation potential [27,28] and the DZV++(3*d*, 1*p*) basis set. These calculations were carried out using GAMESS [29]. The optimized bond lengths are presented in Table I.

We used the Schwinger multichannel (SMC) method implemented with pseudopotentials (SMCPP) in both the static-exchange (SE) and static exchange plus polarization (SEP) approximations to calculate the elastic integral, differential and momentum transfer cross sections for energies up to 30 eV. The SMC method [30,31] is a variational approach to compute the scattering amplitude for electron scattering by molecules. This method and its recent implementations have been described elsewhere [32] and here we will only describe the key aspects of the method which are necessary for the present application.

In the SMC method, the scattering amplitude is given by

$$f(\vec{k}_f, \vec{k}_i) = -\frac{1}{2\pi} \sum_{m,n} \langle S_{\vec{k}_f} | V | \chi_m \rangle (d^{-1})_{mn} \langle \chi_n | V | S_{\vec{k}_i} \rangle, \quad (1)$$

where

$$d_{mn} = \langle \chi_m | A^{(+)} | \chi_n \rangle \quad (2)$$

and

$$A^{(+)} = \frac{\hat{H}}{N+1} - \frac{(P\hat{H} + \hat{H}P)}{2} + \frac{(PV + VP)}{2} - VG_p^{(+)}V. \quad (3)$$

In the expressions above, $\{|\chi_m\rangle\}$ are $(N+1)$ -electron trial configuration-state functions (CSFs), which are spin-adapted (doublet) products of target states with one-particle scattering orbitals, P is a projector onto the energy-allowed target electronic channels, $G_p^{(+)} = PG_0^{(+)}$ is the free particle Green's function $G_0^{(+)}$ projected onto the P space, V is the interaction potential, \vec{k}_i and \vec{k}_f

TABLE I. Optimized molecular bond lengths (in angstroms) for $X(CH_3)_4$ ($X = C, Si, Ge$).

Molecule	R_{X-C}	R_{C-H}
$C(CH_3)_4$	1.538	1.097
$Si(CH_3)_4$	1.884	1.098
$Ge(CH_3)_4$	1.967	1.096

TABLE II. Exponents of the uncontracted basis functions for C, Si, and Ge.

Type	C	Si	Ge
<i>s</i>	12.49628	6.143172	4.557567
<i>s</i>	2.470286	3.207261	1.208832
<i>s</i>	0.614028	1.723970	0.603703
<i>s</i>	0.184028	0.176634	0.173594
<i>s</i>	0.039982	0.037088	0.048634
<i>p</i>	5.228869	1.197710	1.677720
<i>p</i>	1.592058	0.436407	0.270291
<i>p</i>	0.568612	0.192513	0.091598
<i>p</i>	0.210326	0.086630	0.034666
<i>p</i>	0.072250	0.036577	0.011682
<i>d</i>	1.794795	1.061585	0.475112
<i>d</i>	0.420257	0.303480	0.195662
<i>d</i>	0.101114	0.103047	0.036696

are the incident and scattered electron wave vectors, $\hat{H} = E - H$ is the total collision energy minus the $(N+1)$ -electron Hamiltonian in the fixed nuclei approximation ($H = H_0 + V$), and $|S_{\vec{k}_i, \vec{k}_f}\rangle$ is the solution of the unperturbed Hamiltonian H_0 being the product of a target state and a plane wave.

For the calculations carried out in the SE approximation, the CSFs are constructed as

$$|\chi_m\rangle = \mathcal{A}|\Phi_1\rangle \otimes |\varphi_m\rangle \quad (4)$$

where $|\Phi_1\rangle$ is the Hartree-Fock target ground state, $|\varphi_m\rangle$ is a scattering orbital, and \mathcal{A} is the antisymmetrization operator. In the SEP approximation, the SE set is enlarged by including CSFs constructed as

$$|\chi_{mn}\rangle = \mathcal{A}|\Phi_m\rangle \otimes |\varphi_n\rangle, \quad (5)$$

where $|\Phi_m\rangle$ are N -electron Slater determinants obtained by performing single (virtual) excitations of the target. In the present calculations, we considered excitations from the occupied (hole) orbitals to a set of unoccupied (particle) orbitals. $|\varphi_n\rangle$ is also a scattering orbital and \mathcal{A} is the antisymmetrizer.

The ground state of each target was described in the Hartree-Fock approximation at the optimized geometry presented in Table I. The core electrons of the heavy atoms were replaced by the norm-conserving pseudopotentials of Bachelet, Hamann, and Schlüter [33]. The basis set employed to describe the valence electrons on this heavy atoms have $5s5p3d$ uncontracted functions, generated according to Bet-

TABLE III. Exponents and coefficients of the basis functions for the hydrogen atom.

Type	Exponent	Coefficient
<i>s</i>	13.361500	0.130844
<i>s</i>	2.0133000	0.921539
<i>s</i>	0.4538000	1.000000
<i>s</i>	0.1233000	1.000000
<i>p</i>	0.7500000	1.000000

TABLE IV. Relation between the symmetries of the T_d and C_{2v} groups.

T_d	C_{2v}
A_1	A_1
A_2	A_2
E	$A_1 + A_2$
T_1	$B_1 + B_2 + A_2$
T_2	$A_1 + B_1 + B_2$

tega *et al.* [34] with the exponents shown in Table II. For the H atom we used the $4s/3s$ basis set of Dunning [35] with one additional p -type function, which are shown in Table III. Since the SMC method deals only with Abelian groups, in the SEP approximation our calculations were done according to the C_{2v} group. We present in Tables IV and V the relation between the symmetries of C_{2v} and T_d groups. We also performed additional calculations in the SE approximation considering T_d symmetry, which is possible in this approximation by choosing the scattering orbitals of a given symmetry.

In the SE calculations we used the Hartree-Fock canonical virtual orbitals, while in the SEP calculation we used improved virtual orbitals (IVOs) [36] to represent the particle and scattering orbitals. For each target the IVOs were generated using triplet coupling with the hole made in the highest occupied molecular orbital of the A_1 symmetry. To preserve the degeneracy of the T_d group, in the SEP calculations for $C(\text{CH}_3)_4$ and $\text{Si}(\text{CH}_3)_4$ we used all 16 occupied orbitals as hole orbitals and the first 62 IVOs as particle and scattering orbitals, while in the calculations for $\text{Ge}(\text{CH}_3)_4$ we used all 16 occupied orbitals as hole orbitals and the first 60 IVOs as particle and scattering orbitals. The number of configurations per symmetry used in the SEP calculations, for each molecule, is presented in Table VI.

III. RESULTS AND DISCUSSION

The calculated ICSs for the three molecules are shown in Fig. 2 in both SE and SEP approximations, along with the TCS measured by Stefanowska-Tur and co-workers [25]. For each molecule, the SE ICS presents an enhanced structure that covers the energies from 5.5 to 20 eV. For $C(\text{CH}_3)_4$ there is a little bump at the beginning of this structure, then there is a small decrease at energies around 11 eV and after that the cross section increases again, reaching its maximum of

TABLE V. Relation between the symmetries of the C_{2v} and T_d groups.

C_{2v}	T_d
A_1	$A_1 + T_2 + E$
A_2	$A_2 + T_1 + E$
B_1	$T_1 + T_2$
B_2	$T_1 + T_2$

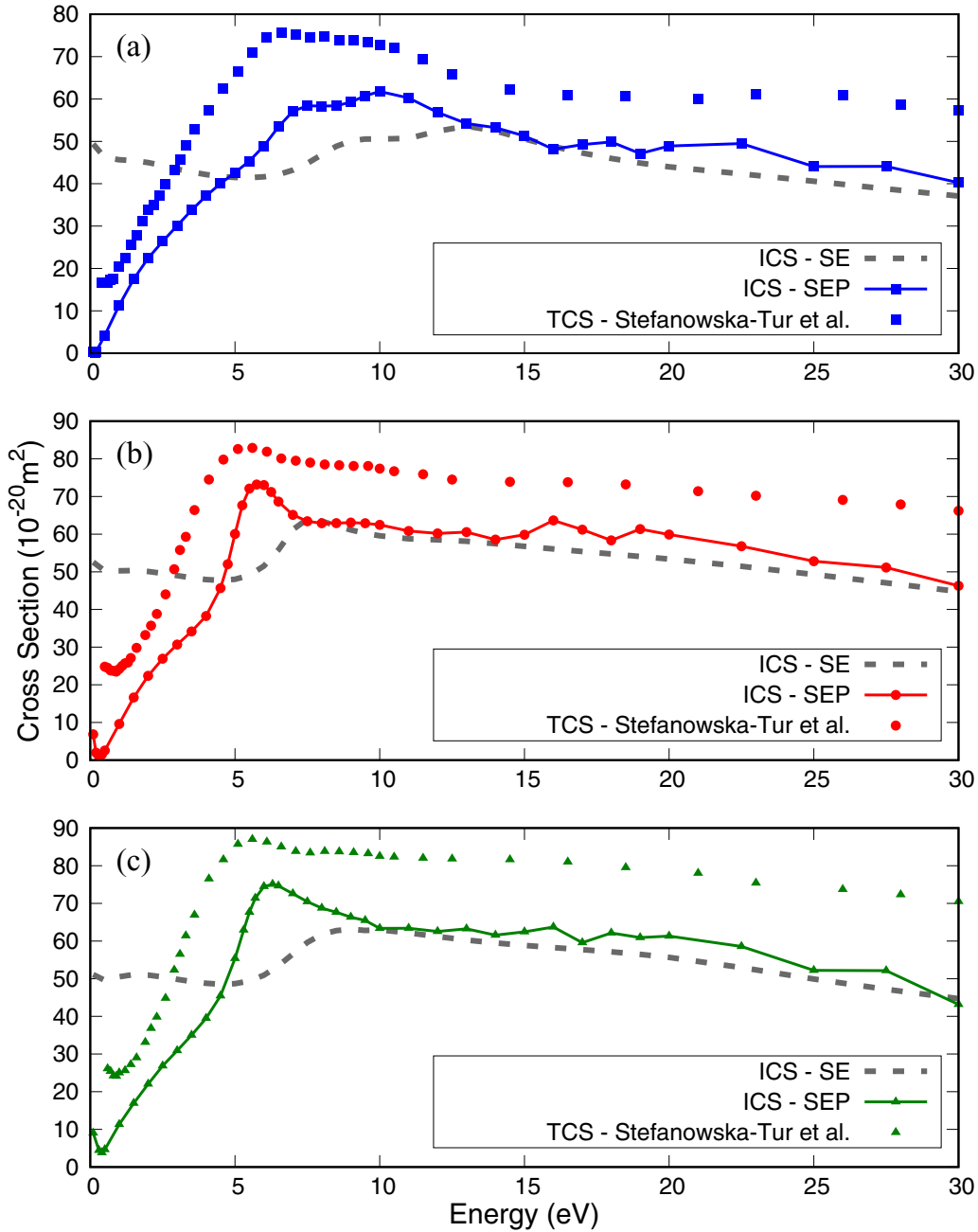


FIG. 2. Integral elastic cross section in the SE and SEP approximations and total cross section from [25] for $\text{C}(\text{CH}_3)_4$ (a), $\text{Si}(\text{CH}_3)_4$ (b), and $\text{Ge}(\text{CH}_3)_4$ (c). See the text for the discussion.

TABLE VI. Number of configurations of each symmetry for $\text{C}(\text{CH}_3)_4$, $\text{Si}(\text{CH}_3)_4$, and $\text{Ge}(\text{CH}_3)_4$ used in the static-exchange plus polarization calculation.

Symmetry	Molecule		
	$\text{C}(\text{CH}_3)_4$	$\text{Si}(\text{CH}_3)_4$	$\text{Ge}(\text{CH}_3)_4$
A_1	15857	15857	15001
A_2	15021	15021	13925
B_1	15436	15436	14460
B_2	15436	15436	14460
Total	61750	61750	57846

$53.6 \times 10^{-20} \text{ m}^2$ at 13 eV. For $\text{Si}(\text{CH}_3)_4$ there is a sharp increase of the cross section at 5 eV until it reaches its maximum value of $64.0 \times 10^{-20} \text{ m}^2$ at 7.5 eV. For $\text{Ge}(\text{CH}_3)_4$ the sharp increase of the cross section occurs at 6 eV until it reaches a maximum of $63.1 \times 10^{-20} \text{ m}^2$ at 9 eV. Aside from that structure, the cross sections obtained in the SE approximation do not show good agreement with the measured TCS [25], especially at low incident energies. This is expected since in this approximation we omit the polarization effects of the molecular target, which is important at low impact energies.

In the SEP ICS the enhanced structure shifts towards lower energies and the behavior of the cross section at low

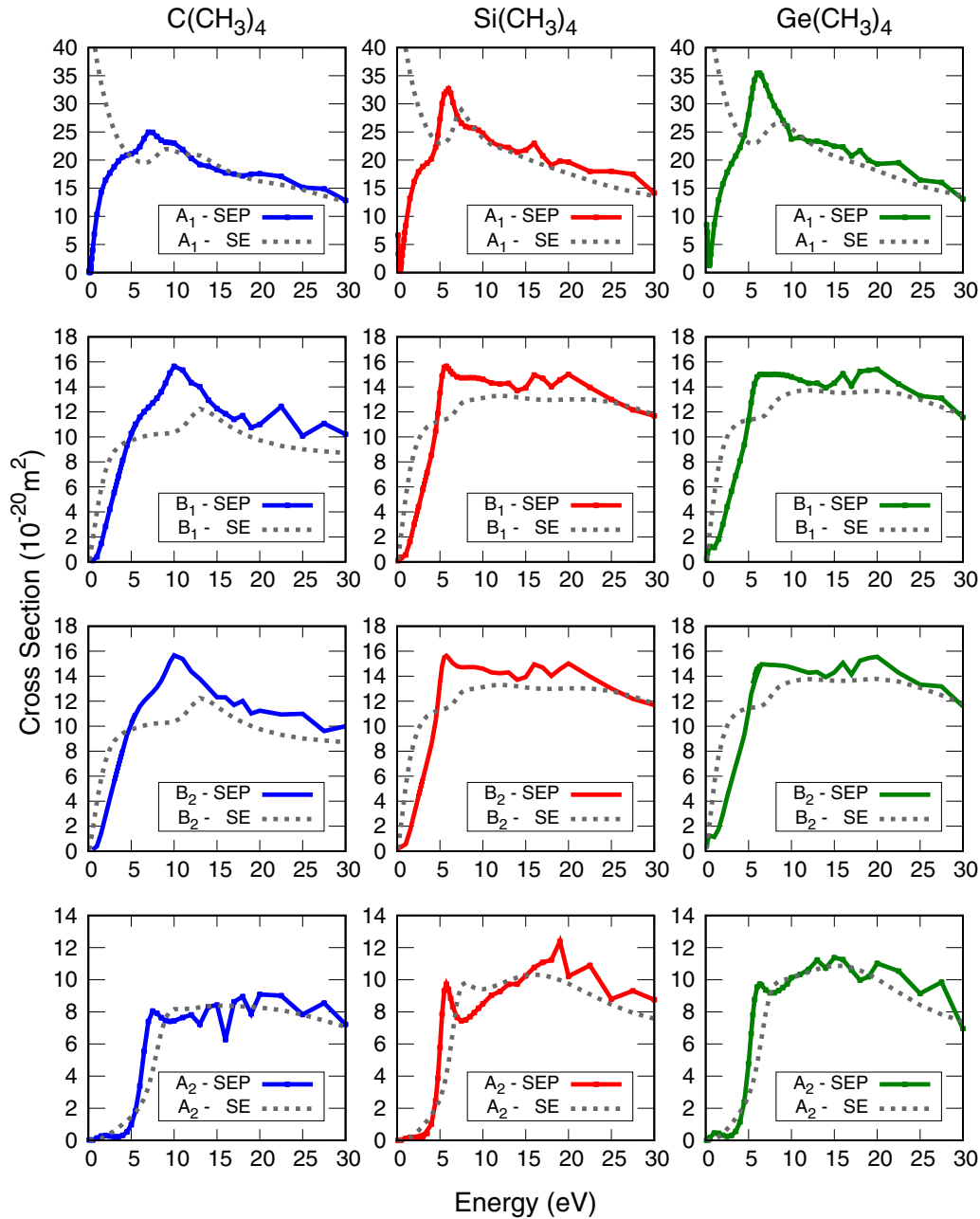


FIG. 3. Symmetry decomposition of the integral cross section in the SE and SEP approximations for $C(CH_3)_4$, $Si(CH_3)_4$, and $Ge(CH_3)_4$ according to the C_{2v} group.

energy changes dramatically. For $C(CH_3)_4$ the structure has a maximum of $61.8 \times 10^{-20} \text{ m}^2$ at 10 eV while the ICS for $Si(CH_3)_4$ and $Ge(CH_3)_4$ have maximum of $73.2 \times 10^{-20} \text{ m}^2$ at 5.8 eV and $74.5 \times 10^{-20} \text{ m}^2$ at 6.3 eV, respectively. One can also observe that for each molecule the shapes of the ICS and the TCS [25] are in good agreement with each other, both theory and experiment having a minimum value at very low energies, the presence of a broad structure located at around the same energy, and a similar behavior at higher energies.

We shown in Fig. 3 the symmetry decomposition of the ICS presented in Fig. 2 for each molecule, according to the C_{2v} group in both SE and SEP approximations. The broad

structure that appears in the integral cross sections of the three systems is due to the superposition of two resonances. In the SEP cross section, the first resonance appears in the A_1 and A_2 symmetries of the C_{2v} point group at around 7.5 eV for $C(CH_3)_4$, 5.8 eV for $Si(CH_3)_4$, and 6.3 eV for $Ge(CH_3)_4$. As shown in Tables IV and V, these two resonance components belong to the twofold degenerate E symmetry of T_d . The second resonance corresponds to structures in the A_1 , B_1 , and B_2 symmetries of the C_{2v} group, at energies slightly higher than the first structure. These three resonances' components belong to the threefold degenerate T_2 symmetry of T_d , as also shown in Tables IV and V. As a result, the broad structure

TABLE VII. Position of the resonances (in eV) of the ICS in the SE and SEP approximations calculated in the present work, in the TCS [25], in ETS experiments [13,23,24], and the calculated MTCS [20]. For the SEP approximation we present the results obtained at the peak of the ICS (SEP-ICS) and from the eigenphase sum analysis (SEP-ESA) and also the width Γ (in eV) obtained according to SEP-ESA.

Molecule	SE	SEP-ICS	SEP-ESA	Γ	TCS	ETS	MTCS
C(CH ₃) ₄	9.5, 13	7.5, 10	7.0, 7.5	2.7, 1.6	6.6 [25]	6.1 [23]	
Si(CH ₃) ₄	7.5	5.8	5.5, 5.1	2.1, 0.7	5.6 [25]	3.9 [23], 3.8 [24], 4.0 [13]	5.8 [20]
Ge(CH ₃) ₄	9.0	6.3	5.7, 5.5	2.6, 0.6	5.6 [25]	3.7 [23], 3.4 [24]	

observed in the ICS shown in Fig. 2 is the superposition of E and T_2 resonances.

The distinction between these two resonances is very clear in the cross sections of C(CH₃)₄, while for Si(CH₃)₄ and Ge(CH₃)₄ this distinction is more difficult to observe, since the positions of the two resonant structures almost overlap. Giordan and Moore [23], through ETS, found that the attachment energy of the lowest unoccupied molecular orbital for C(CH₃)₄ is 6.1 eV, for Si(CH₃)₄ is 3.9 eV, and for Ge(CH₃)₄ is 3.7 eV. Results of ETS experiments made by Modelli *et al.* [24] reported a resonance centered around 3.8 eV for Si(CH₃)₄ and around at 3.4 eV for Ge(CH₃)₄, associated with the capture of the incident electron by the lowest σ^* molecular orbital. In the case of Si(CH₃)₄, the authors assigned the lowest unoccupied molecular orbital (LUMO) and the LUMO+1 to the a_1 and t_2 symmetries, as obtained in an *ab initio* calculation, or to t_2 and a_1 symmetries, according to a semiempirical calculation. Note that the positions of the resonances reported by Modelli *et al.* [24] are in good agreement with the results of Giordan and Moore [23]. Huber *et al.* [13] obtained the electron attachment energies through the vibration excitation function and found a resonant structure centered around 4.0 eV for Si(CH₃)₄. The authors assigned the LUMO to the t_2 symmetry, as obtained in a DFT calculation. Huber *et al.* suggested that the somewhat higher value of this broad structure may indicate that it is in fact a result of the overlap of more than one resonance. Stefanowska-Tur *et al.* [25] concluded that the resonant structure observed in the measured TCS is due to the capture of the incident electron in a molecular orbital of t_2 symmetry only. These results are summarized in Table VII.

Figure 3 also shows that the cross sections for Si(CH₃)₄ and Ge(CH₃)₄ are very similar. Another feature shown in this figure is that the low-energy minimum present in the ICSs of Fig. 2 comes from the A_1 symmetry. The peaks in the cross sections at higher energies are pseudoresonances, which are related to electronic excited channels that are above threshold, but are treated as closed in the present SEP calculations. We can estimate the excitation thresholds through a single configuration interaction calculation using the same single-particle basis, the same orbitals, and the hole-particle excitations as used in the SEP calculation. This would give the spectrum of the electronic excited states associated with the pseudoresonances (we would also need to include the thresholds in the cross section energy grid). We carried out such a calculation using a reduced number of (ten) hole-particle excitations and

obtained for the first excited state 9.8 eV for C(CH₃)₄, 8.9 eV for Si(CH₃)₄, and 8.3 eV for Ge(CH₃)₄. We also performed a full single configuration interaction (FSCI) calculation (with the same single-particle basis used in the SEP calculation) and obtained for the first excited state 9.4, 8.5, and 8 eV for C(CH₃)₄, Si(CH₃)₄, and Ge(CH₃)₄ respectively. As shown in Figs. 2 and 3, the pseudoresonances appear in the cross section of each target above the corresponding threshold. We also show in Table VIII the first six excitation thresholds obtained in a FSCI calculation that are estimates for the pseudoresonances energies.

To explore more precisely the symmetry of the resonances shown in Figs. 2 and 3, we performed a calculation in the T_d point group only in the SE approximation. The results are shown in Fig. 4. For C(CH₃)₄ this analysis shows that the first resonance (around 9.5 eV) belongs to the E symmetry and the second resonance (around 13 eV) belongs to the T_2 symmetry. The same occurs for Si(CH₃)₄ and Ge(CH₃)₄ where the two resonances (centered around 7.5 and 9.0 eV, respectively) appear in the cross sections of the E and T_2 irreducible representations. Therefore, the broad structure that appears in the ICS of all three compounds is in fact the superposition of two resonances, one in the E symmetry and another in the T_2 symmetry. For Ge(CH₃)₄, one can also observe a very broad structure in the A_1 symmetry located at around 10 eV. We also performed the eigenphase sum analysis by fitting the eigenphase sums to a Breit-Wigner profile in order to find the resonance energy and width, and the results are shown in Table VII. In some cases the resonance energy obtained at the peak of the ICS is a little higher than the position obtained from the eigenphase sum.

TABLE VIII. Vertical excitation energies (in eV) for the first six excited states of C(CH₃)₄, Si(CH₃)₄, and Ge(CH₃)₄ obtained at the full single configuration interaction level of approximation.

C(CH ₃) ₄		Si(CH ₃) ₄		Ge(CH ₃) ₄	
State	FSCI	State	FSCI	State	FSCI
1^3T_2	9.399	1^3T_2	8.543	1^3T_2	7.975
1^1T_2	9.834	1^1T_2	8.886	1^1T_2	8.312
2^3T_1	9.896	2^3A_1	9.088	2^3A_1	8.481
3^3A_1	9.985	3^3T_1	9.638	2^1A_1	8.917
2^1T_1	10.494	2^1A_1	9.686	3^3E	9.013
3^1E	10.617	3^1E	10.024	3^1T_1	9.075

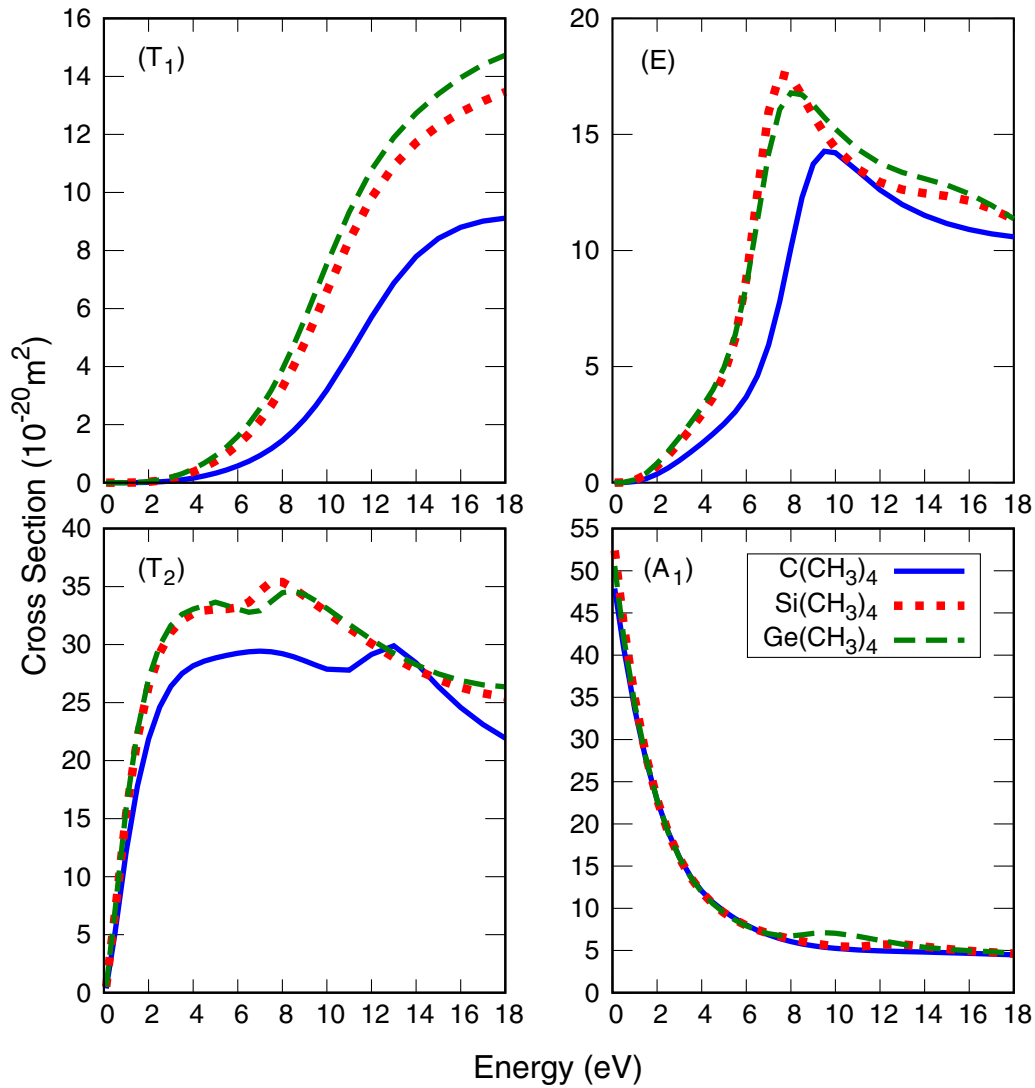


FIG. 4. Symmetry decomposition of the integral cross section obtained in the SE approximation for $C(CH_3)_4$, $Si(CH_3)_4$, and $Ge(CH_3)_4$ according to the T_d group.

Although one may expect that the ICS and the TCS have a similar magnitude at low energies, since the main channel open at this energy range is the elastic channel, this does not occur. We believe that there are more open channels than the elastic one in this energy regime for these molecules. Kawaguchi *et al.* [20] proposed a set of cross section for $Si(CH_3)_4$ where the first vibration channel is open at energies as low as 0.1 eV. In Fig. 5 we present an effective inelastic cross section that is the sum of all the inelastic cross sections presented by Kawaguchi *et al.* [20] except for the ionization cross section, where we have used those from Basner *et al.* [15]. We also show in this figure the ICS calculated in the SEP approximation, the measured TCS from Stefanowska-Tur *et al.* [25], and the sum of the effective inelastic cross section to our ICS. When comparing these data, one can see that the difference in magnitude between the TCS and the ICS diminishes for energies below 15 eV, while the sum

becomes bigger than the TCS for energies above 15 eV. Therefore, we suspect that there are more open channels in the low-energy regime that were not considered in our calculations which contribute to the difference in magnitude between the measured TCS and the calculated ICS. Unfortunately, the lack of data in the literature for $C(CH_3)_4$ and $Ge(CH_3)_4$ makes this interpretation more speculative for these two molecules.

The comparison between the ICSs calculated in this work for all three molecules in the SEP approximation and the measured TCS [25] is presented in Fig. 6. For incident electron energies below 4 eV all three cross sections overlap, except at really low incident energies. For energies higher than 4 eV the cross sections of $Si(CH_3)_4$ and $Ge(CH_3)_4$ almost overlap; the $Ge(CH_3)_4$ cross section being slightly bigger in magnitude than the cross section of $Si(CH_3)_4$. Although the ICS of $C(CH_3)_4$ for energies above 4 eV is lower in magnitude than cross sections of the two other

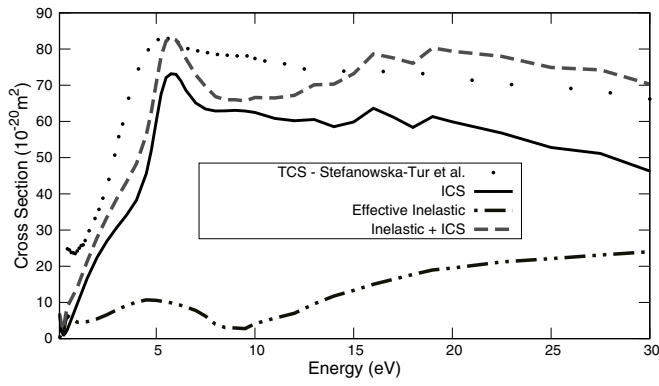


FIG. 5. Set of cross sections for $\text{Si}(\text{CH}_3)_4$. Present integral elastic cross section in the SEP approximation, solid line; total cross section from [25], dots; effective inelastic cross section, that is the sum of all the inelastic cross section presented by Kawaguchi *et al.* [20] and the ionization cross section measured by Basner *et al.* [15], dash-dotted line; sum of the effective inelastic cross section and the integral elastic cross section, dashed line.

systems, the three cross sections have a similar shape. The same comparison can be made when one analyzes the TCS for these three molecules [25], shown in the inset of this figure.

Another interesting feature emerges when one analyzes the *s*-wave scattering of electrons by these three systems. The *s*-wave cross section and the *s*-wave eigenphase are presented in

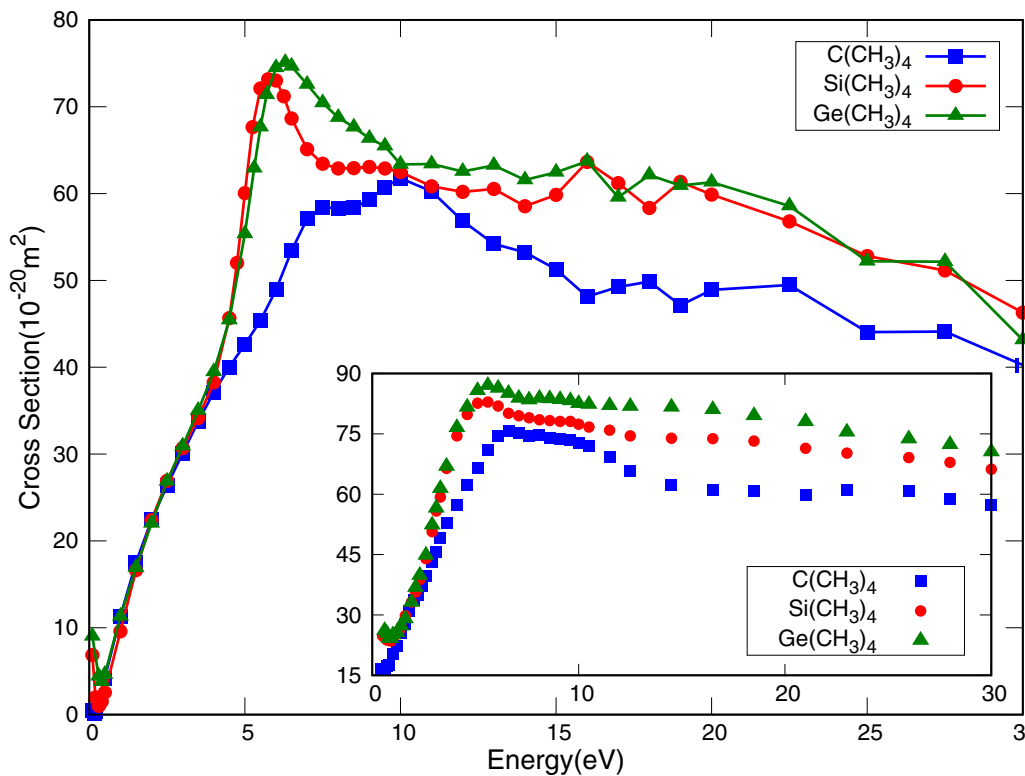


FIG. 6. Comparison between the integral elastic cross section in the SEP approximation for $\text{C}(\text{CH}_3)_4$, $\text{Si}(\text{CH}_3)_4$, and $\text{Ge}(\text{CH}_3)_4$. The inset shows the total cross section for these three molecular targets measured by Stefanowska-Tur *et al.* [25].

Fig. 7. Our calculations show the presence of a RT minimum in the ICS at 0.16 eV for $\text{C}(\text{CH}_3)_4$, 0.32 eV for $\text{Si}(\text{CH}_3)_4$, and 0.40 eV for $\text{Ge}(\text{CH}_3)_4$. A RT minimum around 0.25 eV was observed in the momentum transfer cross section for $\text{C}(\text{CH}_3)_4$ [22] and in the interval between 0.3 and 0.6 eV for $\text{Si}(\text{CH}_3)_4$ [18–20], in agreement with our results.

Figure 8 shows the calculated differential cross sections (DCSs) for the three molecules for the incident energies of 1, 3, 5, 7, 10, 15, 20, 25, and 30 eV. We present only the SEP results. In general the DCSs for $\text{Si}(\text{CH}_3)_4$ and $\text{Ge}(\text{CH}_3)_4$ are similar for all energies. The DCSs for $\text{C}(\text{CH}_3)_4$ at 5 and 7 eV have contribution from the *f*-wave, while the DCSs for $\text{Si}(\text{CH}_3)_4$ and $\text{Ge}(\text{CH}_3)_4$ present a *d*-wave behavior.

Since $\text{Si}(\text{CH}_3)_4$ and $\text{Ge}(\text{CH}_3)_4$ are molecules with industrial interest, in order to present a more complete set of cross sections in Fig. 9 we show our calculated momentum transfer cross section (MTCS) for $X(\text{CH}_3)_4$ ($X = \text{C}, \text{Si}, \text{Ge}$). Along with our results in both SE and SEP approximations, we also present the MTCS calculated by Kawaguchi *et al.* [20] for $\text{Si}(\text{CH}_3)_4$. The RT minimum is also present in the MTCS for all three molecules. Comparing our results for $\text{Si}(\text{CH}_3)_4$ to those of Kawaguchi *et al.* [20] we observe that the position of the RT minimum and the maximum on the cross section agree very well, but there are some differences in magnitude. It is worthwhile to mention that Kawaguchi *et al.* [20] estimated the MTCS for energies below 100 eV in order to obtain the electron drift velocity and the longitudinal diffusion coefficient in agreement with measured data [17].

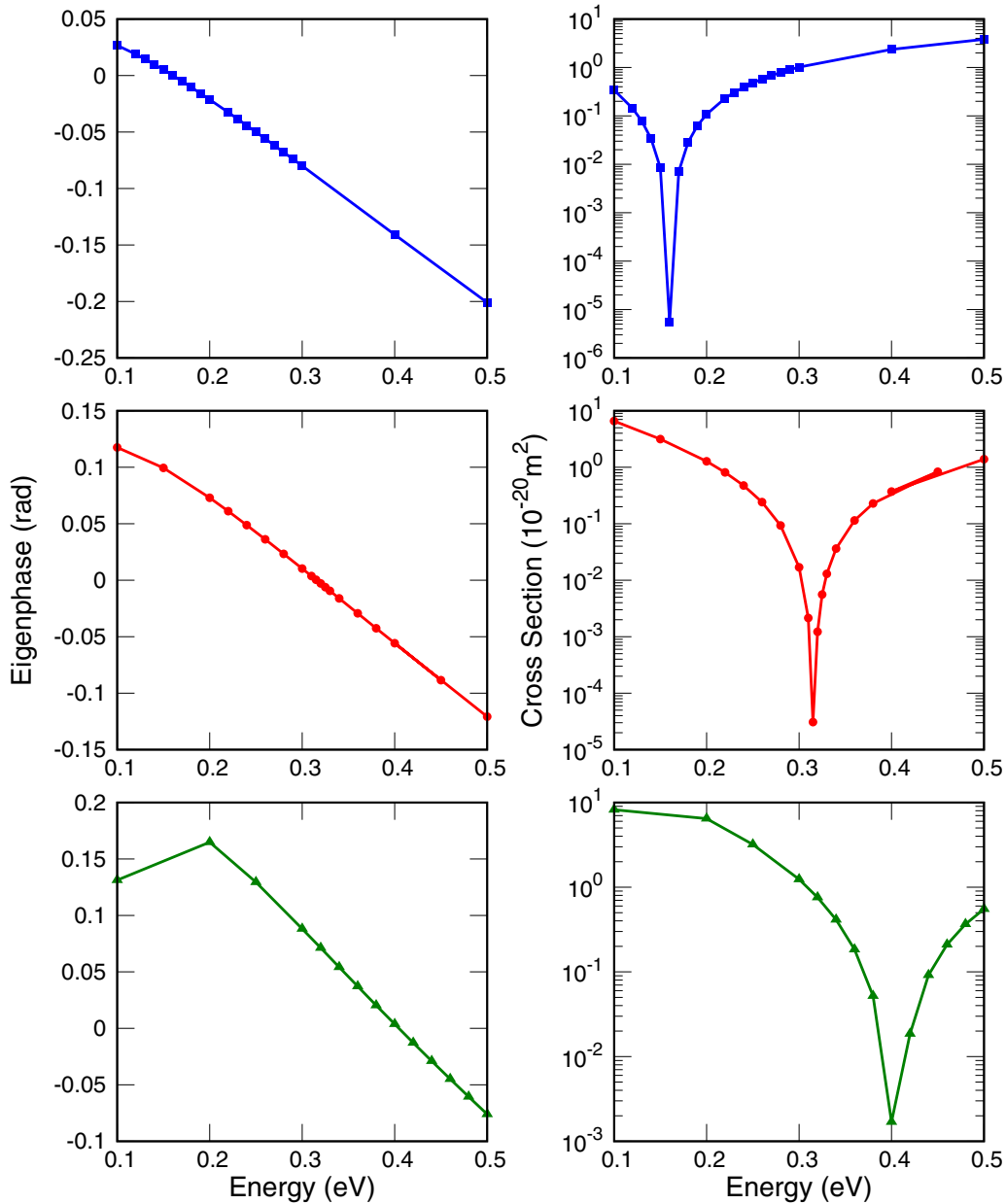


FIG. 7. s -wave eigenphase (left panel) and the s -wave cross section (right panel) in the SEP approximation. $C(CH_3)_4$ molecule, upper panels; $Si(CH_3)_4$, middle panels; $Ge(CH_3)_4$ molecule, lower panels.

IV. CONCLUSION

Elastic ICS, DCS, and MTCS for $C(CH_3)_4$, $Si(CH_3)_4$, and $Ge(CH_3)_4$ have been calculated with the SMCPP method. In the SEP approximation, the ICS of all three molecules present a broad structure in the energy regime from 5 to 15 eV, which is superposition of E and T_2 resonances. While the cross sections for all three molecules have a similar behavior at energies below 4 eV, for energies above 4 eV the ICS for $Si(CH_3)_4$ and $Ge(CH_3)_4$ are very similar and are above the ICS of $C(CH_3)_4$. Our calculated ICSs have a qualitative similar behavior than the TCS measured by Stefanowska-Tur *et al.* [25] and the difference in magnitude at low energies is

attributed to open channels that are not considered in our calculations. A RT minimum was observed in the cross section of $C(CH_3)_4$ at 0.16 eV, of $Si(CH_3)_4$ at 0.32 eV, and of $Ge(CH_3)_4$ at 0.40 eV, and the results for $C(CH_3)_4$ and $Si(CH_3)_4$ are in good agreement with results from previous works [18–20,22]. The MTCS for all three molecules were also presented. The comparison between our MTCS for $Si(CH_3)_4$ and that calculated by Kawaguchi *et al.* [20] shows good agreement in the position of the resonance and in the RT minimum, but they differ in magnitude at higher energies. More theoretical and experimental studies are needed for these molecular targets.

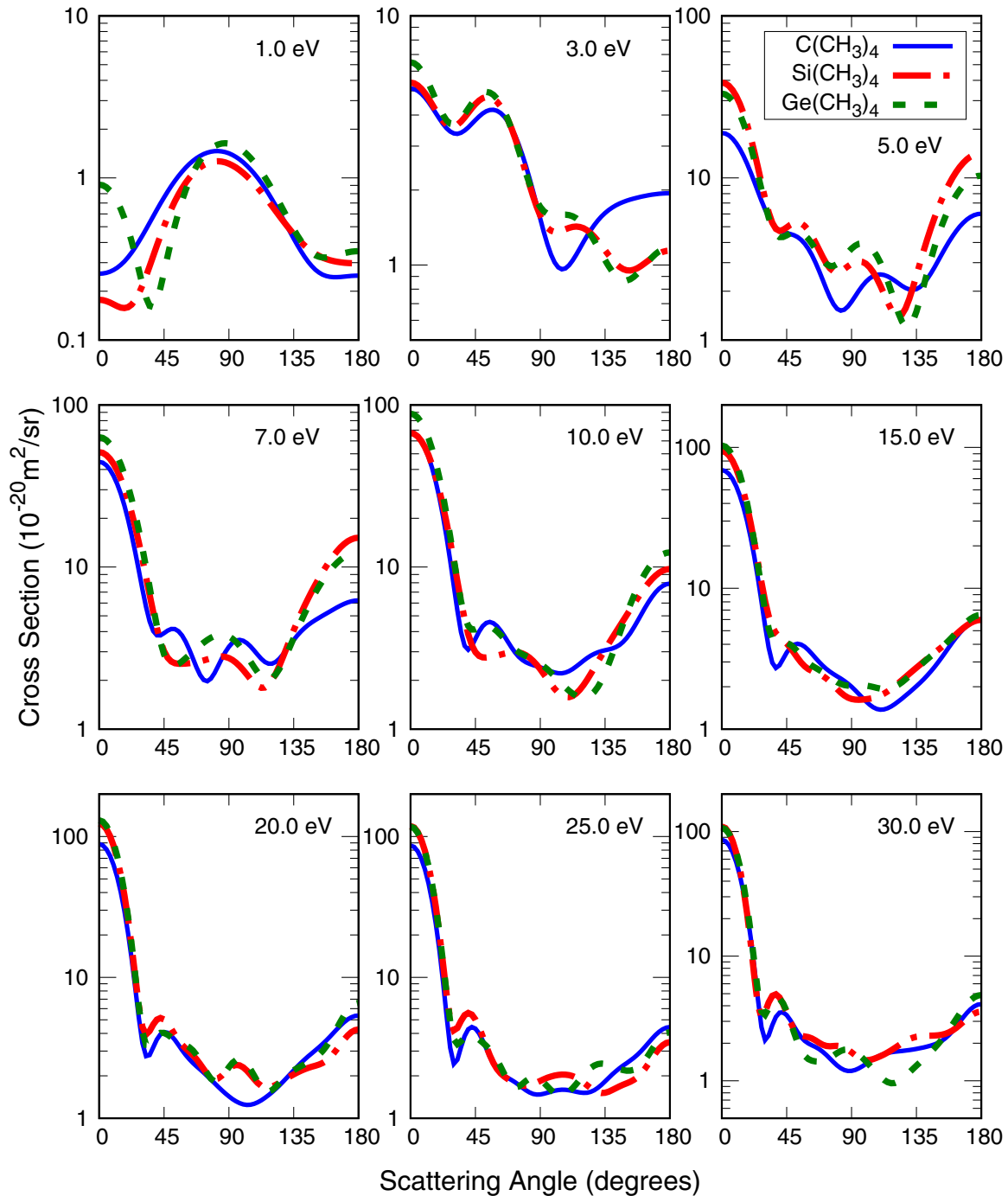


FIG. 8. Differential elastic cross sections in the SEP approximation for $C(CH_3)_4$ (full line), $Si(CH_3)_4$ (dash-dotted line), $Ge(CH_3)_4$ (dashed line) at selected impact energies.

ACKNOWLEDGMENTS

The authors acknowledge support from Brazilian agency Conselho Nacional de Desenvolvimento Científico e Tecnológico (CNPq). G.M.M. and M.H.F.B. also acknowledge support from Brazilian agency Coordenação de Aperfeiçoamento de Pessoal de Nível Superior (CAPES). M.H.F.B.

also acknowledges support from FINEP (under project CT-Infra). The authors acknowledge computational support from Professor Carlos M. de Carvalho at DFis-UFPR and at LCPAD-UFPR. G.M.M. and M.H.F.B. also acknowledge computational support from CENAPAD-SP. The authors would like to thank Professor Stephen Buckman for invaluable discussions and suggestions concerning this work.

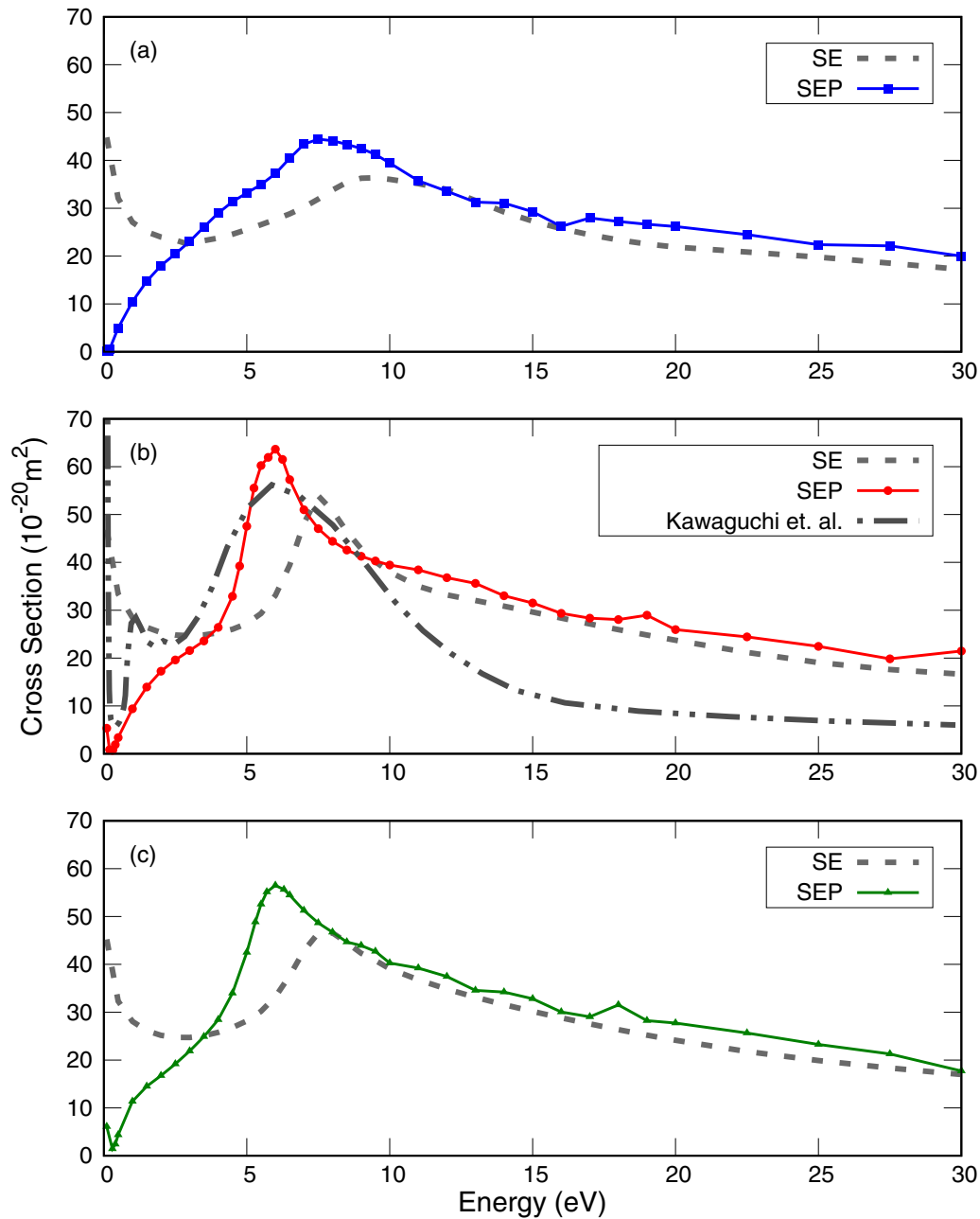


FIG. 9. Calculated momentum transfer cross section in the SE and SEP approximations for $\text{C}(\text{CH}_3)_4$ (a), $\text{Si}(\text{CH}_3)_4$ (b), and $\text{Ge}(\text{CH}_3)_4$ (c). We also show the momentum transfer cross section obtained by Kawaguchi *et al.* [20] for $\text{Si}(\text{CH}_3)_4$ for comparison.

-
- [1] N. J. Mason, *J. Phys.: Conf. Ser.* **565**, 012001 (2014).
 [2] B. Boudaïffa, P. Cloutier, D. Hunting, M. A. Huels, and L. Sanche, *Science* **287**, 1658 (2000).
 [3] L. Sanche, *Nature (London)* **461**, 358 (2009).
 [4] M. C. Boyer, N. Rivas, A. A. Tran, C. A. Verish, and C. R. Arumainayagam, *Surf. Sci.* **652**, 26 (2016).
 [5] K. E. Shulenberger, J. L. Zhu, K. Tran, S. Abdullahi, C. Belvin, J. Lukens, Z. Peeler, E. Mullikin, H. M. Cumberbatch, J. Huang, K. Regovich, A. Zhou, L. Heller, M. Markovic, L. Gates, C. Buffo, R. Tano-Menka, C. R. Arumainayagam, E. Böhler, P. Swiderek, S. Esmaili, A. D. Bass, M. Huels, and L. Sanche, *ACS Earth Space Chem.* **3**, 800 (2019).
 [6] M. Huth, F. Porrati, and O. V. Dobrovolskiy, *Microelectron. Eng.* **185**, 9 (2017).
 [7] W. N. G. Hitchon, *Plasma Processes for Semiconductor Fabrication* (Cambridge University Press, Cambridge, 1999).
 [8] A. Perentes and P. Hoffmann, *Chem. Vap. Deposition* **13**, 176 (2007).
 [9] M. Kihel, S. Sahli, A. Zenasni, P. Raynaud, and Y. Segui, *Vacuum* **107**, 264 (2014).

- [10] H.-Y. Wu, C.-H. Hsu, T.-X. Liu, Y.-C. Ou, Y.-H. Hsu, W.-Y. Wu, S.-Y. Lien, and Y.-L. Jiang, *Surf. Coat. Technol.* **376**, 68 (2019).
- [11] P. Kazimierski, *Thin Solid Films* **495**, 144 (2006).
- [12] A. Užupis, J. Tyczkowski, K. Gubiec, S. Tamulevičius, M. Andrulevičius, and M. Pucėta, *Mater. Sci. (Medziagotyra)* **15**, 7 (2009).
- [13] V. Huber, K. R. Asmis, A.-C. Sergenton, M. Allan, and S. Grimme, *J. Phys. Chem. A* **102**, 3524 (1998).
- [14] H. Faidas, L. G. Christophorou, D. L. McCorkle, and J. G. Carter, *Nucl. Instrum. Methods Phys. Res. A* **294**, 575 (1990).
- [15] R. Basner, R. Foest, M. Schmidt, F. Sigeneger, P. Kurunczi, K. Becker, and H. Deutsch, *Int. J. Mass Spectrom. Ion Processes* **153**, 65 (1996).
- [16] K. N. Joshipura, B. G. Vaishnav, and S. Gangopadhyay, *Int. J. Mass Spectrom.* **261**, 146 (2007).
- [17] K. Yoshida, S. Mori, Y. Kishimoto, H. Ohuchi, H. Hasegawa, M. Shimozuma, and H. Tagashira, *J. Phys. D: Appl. Phys.* **38**, 1918 (2005).
- [18] M.-C. Bordage, *Plasma Sci. Technol.* **9**, 756 (2007).
- [19] P. X. Hien, D. A. Tuan, and B.-H. Jeon, *J. Korean Phys. Soc.* **61**, 62 (2012).
- [20] S. Kawaguchi, K. Takahashi, K. Satoh, and H. Itoh, *Plasma Sources Sci. Technol.* **26**, 054001 (2017).
- [21] R. T. Sugohara, M.-T. Lee, G. L. C. de Souza, M. G. P. Homem, and I. Iga, *Phys. Rev. A* **84**, 062709 (2011).
- [22] D. McCorkle, L. Christophorou, D. Maxey, and J. Carter, *J. Phys. B: At. Mol. Phys.* **11**, 3067 (1978).
- [23] J. C. Giordan and J. H. Moore, *J. Am. Chem. Soc.* **105**, 6541 (2007).
- [24] A. Modelli, D. Jones, L. Favaretto, and G. Distefano, *Organometallics* **15**, 380 (1996).
- [25] S. Stefanowska-Tur, P. Możejko, E. Ptasińska-Denga, and C. Szmytkowski, *J. Chem. Phys.* **150**, 094303 (2019).
- [26] B. M. Bode and M. S. Gordon, *J. Mol. Graph. Mod.* **16**, 133 (1998).
- [27] A. D. Becke, *J. Chem. Phys.* **98**, 1372 (1993).
- [28] P. J. Stephens, F. Devlin, C. Chabalowski, and M. J. Frisch, *J. Chem. Phys.* **98**, 11623 (1994).
- [29] M. W. Schmidt, K. K. Baldridge, J. A. Boatz, S. T. Elbert, M. S. Gordon, J. H. Jensen, S. Koseki, N. Matsunaga, K. A. Nguyen, S. J. Su, T. L. Windus, M. Dupuis, and J. A. Montgomery, *J. Comput. Chem.* **14**, 1347 (1993).
- [30] K. Takatsuka and V. McKoy, *Phys. Rev. A* **24**, 2473 (1981).
- [31] K. Takatsuka and V. McKoy, *Phys. Rev. A* **30**, 1734 (1984).
- [32] R. F. da Costa, M. T. do N. Varella, M. H. F. Bettega, and M. A. P. Lima, *Eur. Phys. J. D* **69**, 159 (2015).
- [33] G. B. Bachelet, D. R. Hamann, and M. Schlüter, *Phys. Rev. B* **26**, 4199 (1982).
- [34] M. H. F. Bettega, A. P. Natalense, M. A. P. Lima, and L. G. Ferreira, *Int. J. Quantum Chem.* **60**, 821 (1996).
- [35] T. H. Dunning, Jr., *J. Chem. Phys.* **53**, 2823 (1970).
- [36] W. J. Hunt and W. A. Goddard III, *Chem. Phys. Lett.* **3**, 414 (1969).